

Tailoring Porous Silica Films through Supercritical Carbon Dioxide Processing of Fluorinated Surfactant Templates

Kaustav Ghosh,[†] Sandhya M. Vyas,[‡] Hans-Joachim Lehmler,[‡] Stephen E. Rankin,[†] and Barbara L. Knutson^{*,†}

Department of Chemical and Materials Engineering, University of Kentucky, Lexington, Kentucky 40506-0046, and Department of Occupational and Environmental Health, University of Iowa, Iowa City, Iowa 52242-5000

Received: August 31, 2006; In Final Form: November 5, 2006

The tailoring of porous silica thin films synthesized using perfluoroalkylpyridinium chloride surfactants as templating agents is achieved as a function of carbon dioxide processing conditions and surfactant tail length and branching. Well-ordered films with 2D hexagonal close-packed pore structure are obtained from sol-gel synthesis using the following cationic fluorinated surfactants as templates: 1-(3,3,4,4,5,5,6,6,7,7,8,8,8-tridecafluoro-octyl)pyridinium chloride (HFOPC), 1-(3,3,4,4,5,5,6,6,7,7,8,8,8-dodecafluoro-7-trifluoromethyl-octyl)pyridinium chloride (HFDoMePC), and 1-(3,3,4,4,5,5,6,6,7,7,8,8,9,9,10,10,10-heptadecafluoro-decyl)pyridinium chloride (HFDePC). Processing the sol-gel film with CO₂ (69–172 bar, 25 and 45 °C) immediately after coating results in significant increases in pore diameter relative to the unprocessed thin films (increasing from 20% to 80% depending on surfactant template and processing conditions). Pore expansion increases with CO₂ processing pressure, surfactant tail length, and surfactant branching. The varying degree of CO₂ induced expansion is attributed to the solvation of the “CO₂-philic” fluorinated tail and is interpreted from interfacial behavior of HFOPC, HFDoMePC, and HFDePC at the CO₂-water interface.

Introduction

Surfactant-templated mesoporous thin films have generated much interest because of their broad range of potential applications in membrane separation, adsorption, catalysis, biomimetics, and chemical and optical sensors.^{1–9} Recently, synthesized ultralow-*k* dielectric trimethylsilylated mesoporous silica thin films and cross-linked methylsilsesquioxane low-*k* dielectric thin films with high mechanical strength have also found application in the microelectronics industry as insulator metal interconnects.^{10,11} The evaporation induced self-assembly (EISA) process for synthesizing surfactant-templated films permits control of the final mesostructure through a variety of parameters such as initial sol composition, pH, aging time, and relative humidity.^{12–16} Tailoring the pore size and structure of surfactant-templated thin films, while maintaining their narrow pore size distribution and large surface area, will increase their potential applications, as demonstrated for tailored mesoporous silica powders in chromatographic and electrode applications.^{17,18}

Porous silica film synthesis by EISA is initiated by coating a substrate with a dilute solution of the surfactant and silica precursor. Evaporation drives the concentration of the surfactant above the critical micelle concentration (cmc). Through a co-assembly process, the hydrolyzed silica precursors associate with the hydrophilic head groups of the surfactants and the hydrophobicity of the surfactant tail drives the formation of micelles. Further solvent evaporation results in a co-assembled mesophase. The precursor then polymerizes to form a solid silica network in the aqueous portions of the surfactant mesophase, and upon subsequent removal of the surfactant, a templated porous silica material is obtained. The most common technique

for tailoring pore size is the introduction of an inert swelling agent directly during the formation of the co-assembled micelle. Hydrocarbon swelling agents (e.g., polypropylene oxide, dodecane, and mesitylene) either solubilize within the tail of traditional hydrocarbon surfactant templates or form an inner core surrounded by a layer of surfactant molecules.^{19–23} When pore expansion occurs through the formation of an inner core rich in the swelling agent, progressive solvent addition can lead to variability in the final pore size. The addition of too much swelling agent can cause complete transition to a new mesophase or loss of long-range order.^{19,21,24}

The tunable solvent strength of compressed and sc (supercritical) CO₂ ($T_c = 31.1$ °C, $P_c = 73.8$ bar) suggests its use for the controlled expansion of pores formed by surfactant templating. Compressed and sc CO₂ has processing advantages relative to organic solvents; it possesses a high diffusivity while also being nonflammable, nontoxic, environmentally acceptable, and inexpensive. The ability of CO₂ to expand mesoporous silica pores has been demonstrated for hydrocarbon copolymer templates (P123, P85, and F127) of mesoporous silica powders.^{25,26} The dilation of hydrocarbon surfactant templates by CO₂ has also been used to infuse reactive precursor into hydrocarbon-based nanocast templates²⁷ and to introduce a gold nanocrystal dispersion into the cylindrical pores of mesoporous silica.²⁸ More recently, we have demonstrated the ability to swell the pores of fluorinated surfactant (HFDePC) templated silica films using CO₂ processing.²⁹ A 90% increase in pore diameter was observed for films processed in sc CO₂ at 172 bar and 45 °C prior to surfactant extraction. In comparison, pressures as great as 482 bar were required to achieve a pore expansion of 54% in silica templated with a hydrocarbon surfactant (Pluronic copolymer, P123).²⁵

The dramatic pore expansion achieved in fluorinated surfactant templated silica suggests a favorable penetration of CO₂

* Corresponding author. Phone: 859-257-5715. Fax: 859-323-1929. E-mail: bknutson@engr.uky.edu.

[†] University of Kentucky.

[‡] University of Iowa.

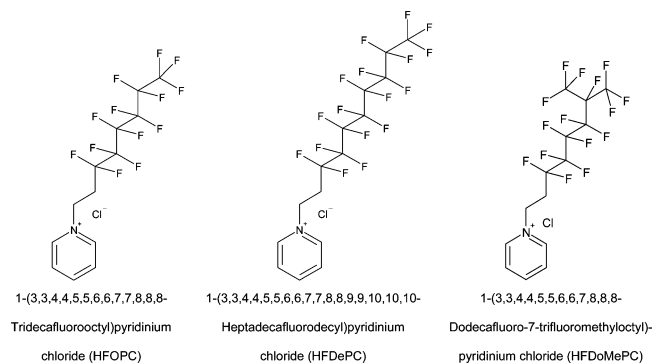


Figure 1. Schematic of the homologous series of perfluoroalkylpyridinium chloride surfactants.

molecules into the fluorinated tails compared to hydrocarbon surfactants. Indeed, many fluorinated moieties have been identified as “CO₂-philic” based on their high solubility in CO₂, and their weak dispersion forces, which are similar to that of CO₂.^{30,31} CO₂ processing of fluorinated surfactant-templated materials has the potential to combine the high degree of solvation of fluorinated tails with the tunable solvent strength of CO₂ to achieve a broad range of pore sizes in nanoporous ceramics. The high diffusivity of sc CO₂ suggests its effective transport into the surfactant tails compared to traditional organic solvents, a property that has already been exploited in the functionalization of mesoporous ceramics.^{32–34}

CO₂ solvation of surfactant templates leading to pore expansion in mesoporous silica draws many analogies to the formation and swelling of self-assembled aggregates (e.g., micelles) in CO₂. Reverse microemulsion behavior in CO₂ has been the focus of numerous investigations because the aqueous core provides a polar environment for organic and enzymatic reactions,^{35,36} extraction,³⁷ nanoparticle syntheses,^{38,39,40} and green applications of carbon dioxide technology.⁴¹ The weak solvation of traditional hydrocarbon surfactant tails by CO₂ is not sufficient to promote CO₂-continuous microemulsion formation. The design of fluorinated and CO₂-philic surfactants for reverse microemulsion formation and the subsequent swelling behavior of micellar systems have provided a great deal of insight into the penetration of CO₂ molecules into the surfactant tail region.^{42–45} The emulsion and microemulsion formation behavior of a series of surfactants and block copolymers has been correlated with interfacial tension (IFT) at the CO₂-water interfaces.^{46–49} Low IFT values are required for reverse microemulsion formation as it decreases the Gibbs free energy penalty associated with the large surface area formed.

In this paper, we report the acid-catalyzed synthesis of mesoporous thin films using a series of perfluoroalkylpyridinium chloride surfactants as pore templates and describe the effect of CO₂ processing on the structure of the thin films. The three surfactant templates, HFOPC, HFDoMePC, and HFDePC (Figure 1), were chosen to systematically study the ability to tailor pore sizes with changes in CO₂ processing conditions, fluorinated template tail length, and surfactant branching. Pore expansion is interpreted from the change in the hydrophilic-CO₂-philic balance (HCB) of each surfactant as a function of processing conditions, as described by the relative solubilities of HFOPC, HFDoMePC, and HFDePC in water and CO₂ and the interfacial activities of the surfactants at the CO₂-water interface.

Materials and Methods

The fluorinated surfactants 1-(3,3,4,4,4,5,5,6,6,7,7,8,8,8-tridecafluorooctyl)pyridinium chloride (HFOPC; C₆F₁₃(CH₂)₂NC₅H₅⁺Cl⁻),

1-(3,3,4,4,4,5,5,6,6,7,7,8,8,9,9,10,10,10-hepta-decafluorodecyl)pyridinium chloride (HFDePC; C₈F₁₇(CH₂)₂NC₅H₅⁺Cl⁻), and 1-(3,3,4,4,4,5,5,6,6,7,8,8,8-dodecafluoro-7-trifluoromethyloctyl)pyridinium chloride (HFDoMePC; (CF₃)₂CFC₄F₈(CH₂)₂NC₅H₅⁺Cl⁻) were synthesized as described previously.⁵⁰ Briefly, for each surfactant, anhydrous pyridine was alkylated with the corresponding 1*H*,*H*,2*H*,2*H*-perfluoroalkyl iodide. The pyridinium iodide was converted into the corresponding chloride by ion exchange chromatography. The purity of all three surfactants was confirmed by mass spectrometry and melting point measurements (as detailed elsewhere).⁵¹ Tetraethoxysilane (TEOS, purity > 99%) was purchased from Gelest. Absolute ethyl alcohol purchased from Aaper Alcohol and Chemical Co. (Shelbyville, KY), deionized ultrafiltered water obtained from Fisher Scientific, and hydrochloric acid (0.1 N standardized solution) obtained from Alfa Aesar were used for thin film synthesis. Carbon dioxide (Coleman grade, 99.99+%) was purchased from Scott Gross Co. (Lexington, KY). Concentrated aqueous HCl (Fisher Scientific) was used for surfactant extraction.

Cross-Polarized Microscopy. Samples of HFDoMePC/H₂O mixtures were observed between crossed polaroids for birefringency and subsequent identification of mesophases at room temperature (23 ± 1 °C). Samples were prepared at four different concentrations (30, 40, 50, and 60 wt %) of HFDoMePC by mixing known amounts of HFDoMePC and water in a vial for 24 h to form a homogeneous mixture. The mixture was then placed on a glass slide in between the channels of a spacer. The spacer was covered by a cover-slip to prevent any evaporation of the sample and allowed to equilibrate for 72 h to form the observed mesophase.

Thin Film Synthesis. Thin porous silica films were synthesized by dip coating on glass slides on the basis of the procedure of Lu et al.⁵² The glass slides were cleaned by treating them in an ultrasonic cleaner and then sequentially rinsing them in water, isopropanol, and acetone. Initially, TEOS, ethanol, water, and HCl (mole ratio 1:3.8:1:5 × 10⁻⁵) were refluxed at 65 °C for 90 min, and a clear solution of partially hydrolyzed silica was formed. Water and HCl were then added in calculated quantities, resulting in a pH of approximately 2 in the final solution, and the mixture was aged at 25 °C for 15 min and then at 50 °C for an additional 15 min. Finally, a solution of the surfactant in ethanol was added to the previously hydrolyzed silica sol under constant stirring. The final mole ratio obtained was 1 TEOS:12 C₂H₅OH:5 H₂O:0.004 HCl:*x* surfactant (*x* varying between 0.15 and 0.21, depending on surfactant). This solution was then dip-coated onto the slides.

Immediately after coating, the thin films were divided into two treatment groups. One treatment group of thin films was pressurized by CO₂ in a 100 mL stainless steel Parr Mini Reactor (rated to 623 K and 207 bar) under controlled temperature and pressure for 72 h. The effects of CO₂ pressure (69–172 bar) and temperature (25 or 45 °C) on the final pore structure were observed. The second treatment group of thin films, which was not processed in CO₂, was dried in an oven at temperature of 25 or 45 °C for 72 h. This ensured uniform thermal conditions for both batches of thin films. Both treatment groups were next heated to 150 °C in vacuum (heating started at 30 °C and oven temperature was ramped by 30 °C every 6 h) to ensure condensation of the silica wall. The surfactant was then extracted from the as-synthesized films by washing twice with acidic ethanol (5 mL of concentrated HCl in 45 mL of EtOH).

Thin Film Characterization. X-ray diffraction patterns were recorded on a Siemens 5000 diffractometer using Cu Kα

radiation ($\lambda = 1.54098 \text{ \AA}$) and a graphite monochromator. Transmission electron microscope (TEM) images were taken with a JEOL 2000FX instrument operating at 200 kV. TEM samples were prepared by scraping the films off the glass substrate and directly depositing them onto a lacey carbon grid. The pore diameters were calculated from the TEM micrographs using ImageJ software, as reported previously.^{29,53} The pore diameters determined by TEM were confirmed by nitrogen sorption measurements (on Micromeritics Tristar 3000 system) for thin films not processed in CO₂, which could readily be prepared in quantities sufficient for nitrogen sorption analysis (> 10 mg). Nitrogen sorption samples were prepared by scraping the films off the glass substrate and degassing at 140 °C for 4 h under flowing nitrogen prior to measurement. The method proposed by Dubinin and Kaganer⁵⁴ was used to calculate pore size for the microporous materials templated by HFOPC while the BJH method with a modified statistical film thickness equation (KJS method)⁵⁵ was used to calculate the pore size distributions for the mesoporous films templated by HFDePC and HFDoMePC.

Interfacial Tension Measurements. Interfacial tensions at the carbon dioxide/water interface in the presence of the three cationic fluorinated surfactants were determined as a function of CO₂ pressure (69–172 bar) at 45 °C. The IFTs were measured at 1.5 wt % surfactant in water, calculated to be above cmc for each surfactant.⁵⁶ IFT analysis was performed using JEFRI high-pressure pendant drop tensiometer (DB Robinson Design & Manufacturing Ltd., Edmonton, Canada) in which the drop phase fluid (surfactant + water) was introduced into a CO₂ continuous phase. A detailed description of the tensiometer is available elsewhere.⁵⁷ An experimental run was initiated by loading CO₂ into the view cell at the desired pressure using a high-pressure syringe pump (ISCO model 500D, Lincoln, NB). Before forming droplets, the aqueous surfactant solution was presaturated with CO₂ at the experimental temperature and pressure. Pendant drops were subsequently formed on the end of the capillary tube (diameter 0.02 cm) by slightly increasing the pressure in the drop phase cylinder relative to the pressure in the view cell. Images of the pendant drop were recorded after approximately 20 min. The interfacial tensions were calculated from analysis of the pendant drop dimensions using a numerical solution to the Laplace equation.^{57,58}

Surfactant Solubility in CO₂. The solubility of the cationic fluorinated surfactants in CO₂ at 25 and 45 °C was examined using a pressure volume temperature (PVT) apparatus (DB Robinson Design & Manufacturing Ltd., Edmonton, Canada), as described previously.⁵⁹ Cloud point pressure was used to indicate the miscibility of surfactants with CO₂.⁵⁹ Pressures of 55–355 bar were traversed at 25 and 45 °C and at concentrations as low as 1 wt % surfactant. The fluorinated surfactants were immiscible with CO₂ at these conditions.

Results and Discussion

Synthesis of Silica Thin Films Templated by Cationic Fluorinated Surfactants. Fluorinated surfactants generally possess higher thermal stability, self-assemble more easily, and form aggregate structures with lower curvature compared to hydrocarbon surfactants.^{56,60} The self-assembly behavior of fluorinated surfactants results in low critical micelle concentrations and low surface tensions, and the formation of fluorinated mesophases with a broader range of structures including novel “intermediate” phases. Our research team has previously demonstrated the homologous series of perfluoroalkylpyridinium chloride surfactants as templates in the base-catalyzed sol–gel

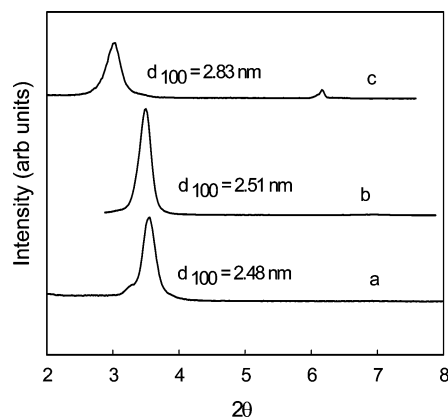


Figure 2. XRD patterns of thin films prepared without CO₂ processing and templated with (a) HFOPC, (b) HFDoMePC, and (c) HFDePC.

synthesis of porous silica powders, resulting in hexagonal close-packed and mesh phase structures,⁵¹ pore sizes in both microporous and mesoporous range,⁵¹ and vinyl functionalized materials with increased accessibility relative to hydrocarbon surfactant (CTAB) templated powders.⁶¹ The synthesis of ceramic thin films by templating with a homologous series of fluorinated surfactants has the potential to control pore size through surfactant tail length and branching, while exploiting the advantageous properties of fluorinated mesophases.

In the present work, the acid-catalyzed syntheses of thin films, the phase behavior of the binary fluorinated cationic surfactant/water system guides the synthesis recipe. Previous syntheses of mesoporous silica films by triblock copolymer templating and CTAB have demonstrated that the final structure of the materials corresponds to the mesophase observed in the surfactant-water phase diagram at equivalent surfactant volume fractions. In calculating equivalent surfactant volume fractions of the sol, the aqueous phase is assumed to comprise the inorganic precursors and the contribution of volatile solvents is neglected.^{62,63} The binary water–surfactant diagrams were obtained from the literature for the surfactants HFOPC⁶⁴ and HFDePC⁶⁰ and volume fractions of 0.7 for HFOPC and 0.67 for HFDePC were selected, corresponding to the center of the hexagonal domain in the phase diagram. A surfactant concentration for formation of hexagonal mesophase in the HFDoMePC/water system was determined as 55 wt % HFDoMePC (volume fraction of 0.64) using cross-polarized microscopy.

The XRD patterns of thin films templated with the three cationic fluorinated surfactants at 45 °C after extraction are presented in Figure 2. Thin films templated with HFOPC and HFDoMePC display one sharp reflection, indicating the formation of ordered structure. The XRD pattern of a film templated with HFDePC shows one sharp reflection corresponding to the (100) plane and a second weaker reflection that can be indexed to the (200) reflection. The presence of ordering after surfactant extraction and position of the two reflections are consistent with the formation of hexagonal structure for the HFDePC templated film; a lamellar structure would have collapsed after surfactant removal. Representative TEM images for all three surfactant templated thin films confirm the presence of well-ordered 2-D hexagonal structure (Figure 3).

The one reflection observed in XRD plots of HFOPC- and HFDoMePC-templated films can then be indexed to the (100) plane of a hexagonal mesostructure. It is worth noting that this is truly an example of evaporation-induced self-assembly; forming ordered bulk materials by polymerization at similar pH and surfactant/silica values has been very difficult due to the

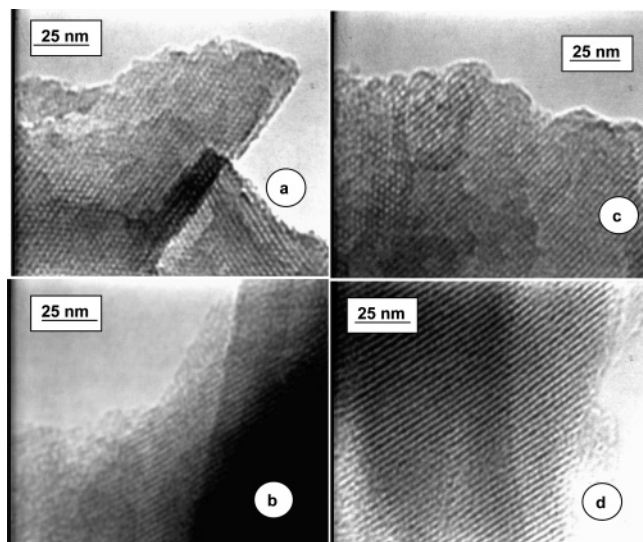


Figure 3. TEM micrographs of thin films prepared without CO₂ processing and templated with (a) HFOPC, (b) HFDoMePC, and (c) HFDePC and (d) for film templated with HFOPC and processed in CO₂ at 172 bar and 45 °C.

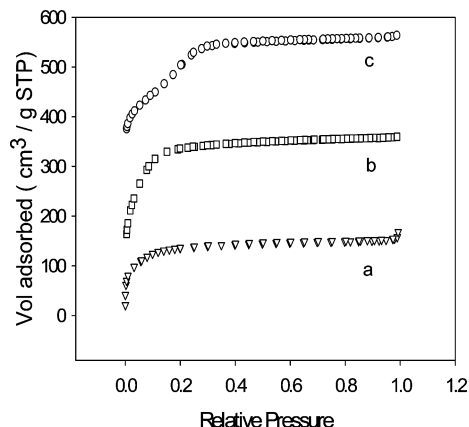


Figure 4. Nitrogen sorption isotherm of thin films prepared without CO₂ processing templated with (a) HFOPC, (b) HFDoMePC, and (c) HFDePC. Open symbols are for adsorption and filled for desorption. The y-axis values have been offset by 130 units (trace b) and by 300 units (trace c) for clarity.

slow assembly of these surfactants in concentrated solution at moderately elevated temperatures.

The nitrogen sorption analysis reveals a type I isotherm for the HFOPC-templated thin film, characteristic of microporous materials (Figure 4), and its pore diameter was estimated as 1.91 nm using the method of Dubinin and Kaganer.⁵⁴ Type IV isotherms, characteristic of mesoporous materials, were observed for films templated with both HFDePC and HFDoMePC. The KJS method (modified BJH method),⁵⁵ applicable to the calculation of physical properties of mesoporous material with uniform cylindrical pores, was used to analyze the N₂ sorption data for both samples. Pore diameters obtained from these N₂ adsorption experiments are 1.98 nm and 2.20 nm for HFDoMePC templated film and HFDePC templated film, respectively. The pore diameters calculated from N₂ sorption measurements compare favorably with those calculated from TEM images (as listed in Table 1). Aging the thin films at 25 °C results in the same hexagonal structure for all three surfactants, with *d*-spacing values and pore sizes similar to values obtained at 45 °C (Table 1).

Templating with a longer-tailed surfactant, the decyl chain surfactant (HFDePC), resulted in a larger pore diameter relative

to the octyl chain surfactant (HFOPC). This is an expected trend because the pore size is determined by the length of the hydrophobic tail group of the surfactant.⁵¹ The tail length for each surfactant molecule was calculated from their optimum configuration using SPARTAN.⁶⁵ The surfactant molecule was first created in an all trans configuration in SPARTAN, and next, an energy minimization was performed on the molecule using the classical MMFF94 force field to obtain the optimum configuration. Finally, the tail length of each surfactant was calculated as the distance between the pyridinium nitrogen atom and the last atom in the tail. HFOPC and a branched version of this surfactant, HFDoMePC (containing an additional CF₂ group), were determined to have similar surfactant tail lengths. However, the pore diameter for the HFDoMePC-templated film is larger compared to that of the HFOPC-templated film, suggesting that branching expands the core of the micelle template.⁵¹ The *d*-spacing values, as calculated from the XRD plots, also increase slightly from the HFOPC-templated film (2.48 nm) to HFDoMePC films (2.51 nm), and are significantly larger for the HFDePC-synthesized film (2.83 nm). The similar trends in pore diameter are expected, as the surfactant chain length contributes to both parameters. However, the *d*-spacing (distance between the (100) planes of the hexagonal close-packed structure) includes both the diameter of the pores and the thickness of the silica walls.

This trend in pore size with surfactant chain length was also observed during the base-catalyzed synthesis of hexagonally ordered silica particles in a homogeneous medium.⁵¹ In that study, the *d*-spacing for the HFOPC templated powders (2.66 nm) was also smaller than both the branched HFDoMePC powders (2.81 nm) and longer chain HFDePC-templated powders (2.96 nm). The larger *d*-spacing for base-catalyzed powders compared to acid-catalyzed films as observed for each template can be attributed to the silica being neutral or slightly positively charged in the acid-catalyzed films, which is expected to lower the aggregation number in the cationic micelles relative to the negatively charged silica present in base-catalyzed synthesis.

Effects of CO₂ Processing on Thin Film Structure. The ability to tailor the pore size of fluorinated surfactant templated thin films by CO₂ processing immediately after coating was examined for this homologous series of cationic surfactants. Varying the properties of the surfactant tail (tail length and branching) and the solvent strength of CO₂ is expected to result in treated thin films having a wide range of pore sizes. CO₂ processing and the resulting penetration of surfactant tail for pore expansion in thin films occur during the modulable steady state (MSS) of the film, a period reached a few seconds after sol coating, when the silica network is not too rigid and the final structure can be modified by external influence.⁶⁶ The higher diffusivity of sc CO₂ is expected to be an advantage compared to organic swelling agents as it allows more rapid penetration into the surfactant tail during silica condensation.

Figure 5 compares XRD plots of thin films templated with HFOPC as a function of CO₂ treatment conditions immediately after coating. At least one sharp peak corresponding to the (100) reflection is observed for all extracted films, indicating that the hexagonal ordering is preserved after CO₂ processing. A decrease in 2θ value for the (100) reflection, corresponding to an increase in *d*-spacing, is evident for CO₂ processed films relative to the unprocessed film. The largest increase in *d*-spacing is observed for the film treated at the highest pressure investigated (2.48 nm for the unprocessed film relative to 3.06 nm for CO₂ processing at 172 bar). Liquid CO₂ (25 °C) and sc

TABLE 1: Summary of d -Spacing and Pore Diameter for Thin Films Templated with Three Different Surfactants as a Function of CO₂ Processing Conditions

CO ₂ -processing conditions	density of CO ₂ (g/mL) ⁸⁷	HFOPC film		HFDePC film		HFDoMePC film	
		d -spacing (nm)	pore diameter ^a (nm)	d -spacing (nm)	pore diameter ^a (nm)	d -spacing (nm)	pore diameter ^a (nm)
unprocessed (45 °C)		2.48	1.91 (0.092)	2.83	2.16 (0.082)	2.51	1.96 (0.086)
unprocessed (25 °C)		2.46	1.90 (0.088)	2.86	2.18 (0.085)	2.53	1.96 (0.084)
69 bar and 45 °C (gas)	0.178	2.78	2.33 (0.086)	3.50	3.06 (0.080)	2.88	2.51 (0.087)
103 bar and 45 °C (sc)	0.544	2.90	2.58 (0.098)	3.94	3.57 (0.084)	3.12	2.84 (0.089)
137 bar and 45 °C (sc)	0.715	2.96	2.69 (0.094)	3.98	3.68 (0.078)	3.21	2.99 (0.082)
172 bar and 45 °C (sc)	0.779	3.06	2.78 (0.090)	4.06	3.86 (0.084)	3.32	3.18 (0.09)
172 bar and 25 °C (liq)	0.894	3.06	2.76 (0.094)	4.05	3.84 (0.082)	3.33	3.17 (0.084)

^a Values in parentheses are standard deviations of pore diameters obtained from 10 different TEM images of the same sample.

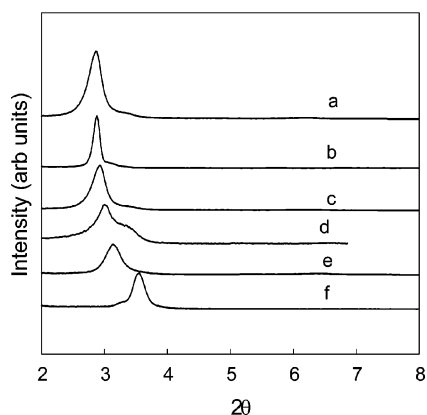


Figure 5. XRD spectra of thin films templated with HFOPC and processed in CO₂ at (a) 172 bar and 45 °C, (b) 172 bar and 25 °C, (c) 137 bar and 45 °C, (d) 103 bar and 45 °C, and (e) 69 bar and 45 °C. (f) Sample not processed in CO₂.

CO₂ (45 °C) treatments at 172 bar result in similar d -spacing values. (Table 1)

TEM images confirm the long-range structure of the CO₂-processed films (representative TEM images are shown in Figure 3) and were used to determine the corresponding pore size (Table 1). The pore diameters measured directly from the TEM images increase with CO₂ pressure. For example, the largest pore diameter observed for the HFOPC templated film is 2.76 nm for CO₂ treatment at 172 bar and 45 °C compared to 1.91 nm for the unprocessed film (Figure 2, Table 1).

The increase in d -spacing (Figure 6a) with CO₂ processing mirrors the increase in pore size (Figure 6b). Both measures of pore expansion increase steadily at lower CO₂ densities, but level off at higher CO₂ density ($\rho_{\text{CO}_2} > 0.6$ g/mL). However, the magnitude of the increase of pore diameter with CO₂ processing (20–80% at the conditions investigated) is significantly greater than the increased d -spacing (10–45%). The difference results from the fact that the thickness of the silica wall, as measured from the difference between the lattice parameter ($a = 2/\sqrt{3} \times d$ -spacing) and the pore diameter, actually decreases between 5% and 25% (depending on CO₂ pressure and surfactant) with increasing pressure. Thus, the observed swelling effect of CO₂ during synthesis is limited to the pores.

The increase in pore expansion with increasing CO₂ pressure (Figure 6) can be interpreted from the driving force for the localization of CO₂ molecules in the surfactant tails. For example, investigations of alkane incorporation within a CTAB (hydrocarbon) micellar system have shown that short alkane swelling agent penetrates the tails of surfactant molecules.^{67,68} In contrast, the free energy of mixing of alkanes in tails is unfavorable for alkanes larger than decane. Hence the larger alkane molecules form a core at the center of the micelle.⁶⁷ CO₂

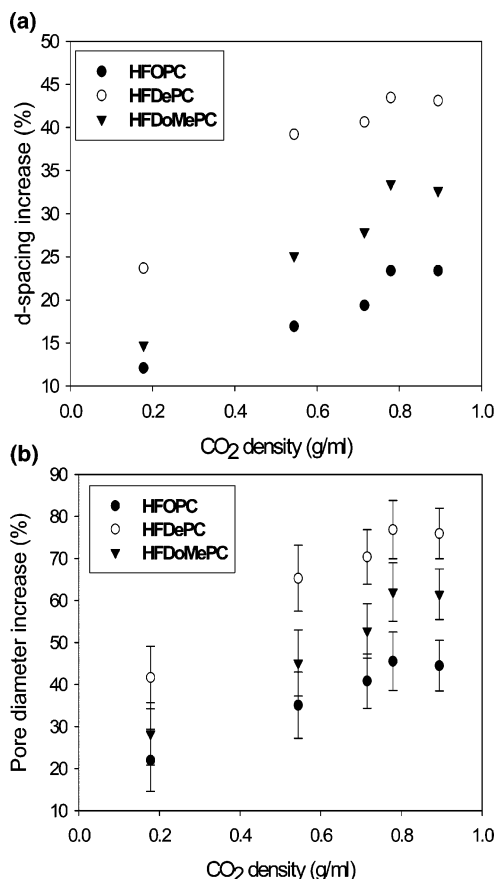


Figure 6. Percentage increase of (a) d -spacing and (b) pore diameter of thin films processed in CO₂ relative to unprocessed films as a function of CO₂ density.

is a small molecule and has a favorable free energy of mixing with the fluorinated tails as indicated by the high solubility of a large number of fluorinated surfactants in CO₂.^{30,31} Thus, CO₂ would be expected to be solubilized in the fluorinated surfactant tails of the templates, as observed in perfluoropolyether surfactant cylindrical micelles.⁶⁹ The larger pore expansion observed with increased CO₂ density is consistent with its increased solvent strength,⁷⁰ resulting in a higher degree of surfactant tail solvation.

Pore expansion reaches a near-constant value at CO₂ densities greater than approximately 0.6 g/mL. Similarly, CO₂ sorption during swelling of bulk and polymer films like poly(methylmethacrylate) (PMMA),^{71–73} polycarbonates (PC),^{71,73} and poly(dimethylsiloxane) (PDMS),^{74,75} and CO₂ solubility in hydrocarbon copolymer agents like poly(propylene oxide) (PPO),²⁶ also increases rapidly at lower pressure and then levels off at higher pressure. Another reason for the observed limit in pore expansion could be that the increased solvent strength with

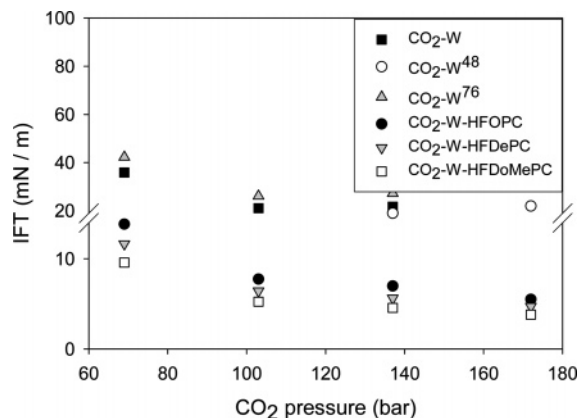


Figure 7. Interfacial tension of all three surfactants at the CO₂–water interface as a function of CO₂ pressure at 45 °C. Scaling on y-axis different above and below the break for clarity. Standard deviations of IFT values from this study ($\pm 4\%$) not shown in figure for clarity. CO₂–water interfacial tensions from this study are compared to those of da Rocha et al.⁴⁸ and Chun and Wilkinson.⁷⁶

increasing CO₂ pressure may be offset by the decreased diffusivity of CO₂ with pressure in supercritical and liquid conditions. An additional explanation is that micelle swelling could be constrained by the silica matrix, which is fixed to a glass slide.

Figure 6 also compares the pore expansion in the silica thin films as a function of surfactant tail length and branching of the template. The film templated with the longer -decyl tail surfactant HFDePC has a greater degree of pore expansion relative to the -octyl tail HFOPC-templated film. CO₂ is capable of solvating the entire length of the fluorinated tail.⁴⁵ Therefore, an increase in number of fluorocarbon groups in the surfactant tail leads to an expected increase in pore expansion by CO₂. The pore expansion for the branched tail surfactant HFDoMePC-templated film is also larger than that of the HFOPC-templated film (Figure 6) even though the unsolvated tail lengths of both surfactants are approximately equal. This result is consistent with previous studies of water-in-CO₂ microemulsions, which have shown that CO₂ better solvates stubby branched surfactant tails relative to straight chain surfactants.⁷⁶

Micelle-Based Interpretation of Pore Expansion. Previous micellization studies in the presence of CO₂ provide insight into the driving force and limitations of CO₂-based pore expansion in templated thin films. Similar to micellization,⁷⁰ the driving forces for pore expansion through surfactant tail solvation by CO₂ can be interpreted as a balance between the favorable free energy of CO₂ penetration of the surfactant tails and the unfavorable free energy penalty associated with micelle swelling. Interfacial tension at the CO₂–water interfaces and solubility studies have been used to interpret properties of self-assembled aggregates such as CO₂-continuous microemulsions as a function of pressure, temperature, and surfactant structure.^{46–49} Figure 7 reports the interfacial tensions (IFTs) of the surfactant templates used in this study, HFOPC, HFDoMePC, and HFDePC, at CO₂–water interfaces relative to pure CO₂–water interface data at 45 °C.^{48,77} The IFT values for all three fluorinated surfactants decrease with an increase in CO₂ pressure and also with an increase of fluorocarbon groups and branching of the tail, as observed in previous studies.^{46,47} The lowest IFT value is observed for the branched chain surfactant, HFDoMePC (3.80 mN/m at 172 bar and 45 °C).

The lowest possible value of IFT for a particular surfactant at CO₂–water interfaces is observed at the most balanced state of hydrophilic–CO₂-philic balance (HCB),⁴⁸ where the surfac-

tant has equal affinity for both phases; inversion of colloidal dispersions between CO₂-in-water and water-in-CO₂ with change in formulation variables (CO₂ pressure, temperature, system pH, and salinity) can occur at this balanced state.^{49,78} In general, the curvature (H) at the CO₂–water interface predicts the existence of colloidal dispersions of CO₂-in-water ($H > 0$) or water-in-CO₂ ($H < 0$) and can be described from the packing parameter.⁴⁹ The distribution of the surfactant between oil and water phases has roughly been used to determine the sign of the curvature (Bancroft's rule),⁷⁹ although Kahlweit suggests that the ratio of cmc's in the two phases (and not the ratio of monomers) is a more accurate predictor of curvature.⁸⁰ Thus, for a surfactant with higher solubility in aqueous phase compared to CO₂, the surfactant lies on the aqueous side of HCB ($HCB > 1$). The homologous series of cationic fluorinated templates in this study was observed to have minimal solubility at concentrations lower than 1 wt % (at 25 and 45 °C and pressures from 55 to 355 bar) in CO₂, while being highly soluble in water (solute concentration > 40 wt %).⁶⁰ Hence, these surfactants lie on the aqueous side of the HCB. The observed decrease in IFT with increasing CO₂ pressure indicates movement toward a more balanced state of HCB (i.e., toward the CO₂-philic side or more favorable penetration of CO₂ molecules in the surfactant tail).⁴⁹

Similarly, the decrease in the IFT at the CO₂–water interface with increasing surfactant tail length is consistent with the larger degree of pore expansion observed for the HFDePC-templated film. However, the IFT values for the branched surfactant, HFDoMePC, are lower than for the -decyl tail surfactant, HFDePC, suggesting that degree of pore expansion for the HFDoMePC-templated film should be greater. This apparent contradiction between IFT values and the observed pore expansion may be explained from the solvation and geometric effects of micelle assembly in CO₂. Branching of the surfactant tail leads to its increased solubility in CO₂ and a concomitant decrease in aqueous solubility,⁷⁶ thereby lowering the interfacial tension for surfactants that favor the aqueous environment over CO₂. A consistent description of the reduced interfacial tension at the CO₂–water interface is the increase in the effective volume of a stubby branched tail with CO₂ penetration of the tail, which minimizes contact between the two immiscible fluids.^{76,81} The geometric dependence of micelle swelling can be described by the penalty in Gibbs free energy during formation of self-assembled aggregates, which is directly related to the creation of interfacial area. For the straight tail surfactant, swelling by CO₂ is limited along the radial direction. However, solvation along the branches of a branched surfactant results in a lesser increase in interfacial area, thus resulting in a smaller free energy penalty. Therefore, the solvation of the branched surfactant can result in a smaller pore diameter increase (expansion is distributed along both branches) compared to the straight chain surfactant, but the CO₂ penetration and hence volume swelling over both branches of HFDoMePC can be greater (consistent with the IFT measurements). CO₂–water interfacial activity and solubility of surfactants in CO₂ can thus be used to interpret the trends in pore expansion as a function of surfactant template structure and CO₂ density.

Conclusions

Nanoporous silica thin films with well ordered hexagonal structure were synthesized by dip-coating using a homologous series of cationic fluorinated surfactants as templating agents under acidic conditions. The nanoporous silica films were processed in CO₂ directly after coating, which resulted in pressure tunable swelling of the CO₂-philic fluorinated templates

leading to thin films with pore diameters in the range of 1.91 (± 0.20) to 3.86 (± 0.20) nm. The pore expansion of thin films increased with an increase in CO₂ pressure and with the tail length of surfactant templates. Branching of the surfactant template resulted in increased swelling of the micelle core, compared to linear tail surfactants, which is consistent with previous studies of CO₂ solvation of fluorinated tails.^{28–30} The long-range ordering of the thin films was retained after pore expansion, unlike some previous investigations using traditional organic solvents as pore swelling agents.^{19,21,24}

Sol-gel processing of templated materials provides the opportunity to capture self-assembled structures into kinetically stable materials.^{82,83} Capturing the effects of CO₂ on self-assembly has practical application (i.e., pore expansion or CO₂-directed self-assembly) and addresses the limited investigations of the effect of CO₂ on surfactant mesophases.^{26,84} In contrast, numerous investigations have focused on the effect of CO₂ on self-assembled aggregates (micelles and microemulsions).^{44–46,85,86} The interpretation of CO₂-induced pore expansion using micelle-based approaches (i.e., interfacial activity and phase behavior, as relevant to the HCB) may provide a systematic guide to design surfactant systems whose resulting co-assembled structures may be altered through CO₂ solvation.

Acknowledgment. The authors would like to acknowledge National Science Foundation NIRT Grant # DMR-0210517 and Kentucky Science and Engineering Foundation Grant KSEF-159-RDE-001 for funding of this research project.

References and Notes

- Bein, T. *Chem. Mater.* **1996**, *8*, 1636.
- Yang, H.; Coombs, N.; Sokolov, I.; Ozin, G. A. *J. Mater. Chem.* **1997**, *7*, 1285.
- Doshi, D. A.; Huesing, N. K.; Lu, M.; Fan, H.; Lu, Y.; Simmons, P. K.; Potter, B. G., Jr.; Hurd, A. J.; Brinker, C. J. *Science* **2000**, *290*, 107.
- Wong, E. M.; Markowitz, M. A.; Qadri, S. B.; Gollodge, S.; Castner, D. G.; Gaber, B. P. *J. Phys. Chem. B* **2002**, *106*, 6652.
- Garnweitner, G.; Smarsly, B.; Assink, R.; Ruland, W.; Bond, E.; Brinker, C. J. *J. Am. Chem. Soc.* **2003**, *125*, 5626.
- Lu, Y.; Yang, Y.; Sellinger, A.; Lu, M.; Huang, J.; Burns, A. R.; Sasaki, D. Y.; Shelnut, J.; Brinker, C. J. *Nature* **2001**, *410*, 913.
- Nicole, L.; Boissière, C.; Grosso, D.; Hesemann, P.; Moreau, J.; Sanchez, C. *Chem. Commun.* **2004**, 2312.
- Fan, H.; Reed, S.; Baer, T.; Schunk, R.; Lopez, G. P.; Brinker, C. J. *Microporous Mesoporous Mater.* **2001**, *44–45*, 625.
- Liu, N. G.; Dunphy, D. R.; Atanassov, P.; Bunge, S. D.; Chen, Z.; Lopez, G. P.; Boyle, T. J.; Brinker, C. J. *Nano Lett.* **2004**, *4*, 551.
- Chen, J. Y.; Pan, F. M.; Chang, L.; Cho, A. T.; Chao, K. J. *J. Vac. Sci. Technol., B* **2005**, *23*, 2034.
- Ciarabella, F.; Jousseau, V.; Maitrejean, S.; Verdier, M.; Remiat, B.; Zenasni, A.; Passemard, G. *Thin Solid Films* **2006**, *495*, 124.
- Grosso, D.; Babonneau, F.; Albouy, P. A.; Amenitsch, H.; Balkenede, A. R.; Brunet-Bruneau, A.; Rivory, J. *Chem. Mater.* **2002**, *2*, 931.
- Besson, S.; Gacoin, T.; Ricolleau, C.; Jacquot, C.; Boileau, J. P. *J. Mater. Chem.* **2003**, *13*, 404.
- Cagnol, F.; Grosso, D.; Soler-Illia, G. J. de A. A.; Crepaldi, E. L.; Babonneau, F.; Amenitsch, H.; Sanchez, C. *J. Mater. Chem.* **2003**, *13*, 61.
- Grosso, D.; Babonneau, F.; Soler-Illia, G. J. de A. A.; Albouy, P. A.; Amenitsch, H. *Chem. Commun.* **2002**, 748.
- Jang, K.; Song, M.; Cho, S.; Kim, J. *Chem. Commun.* **2004**, 1514.
- Ma, Y.; Qi, L.; Ma, J.; Wu, Y.; Liu, O.; Cheng, H. *Colloids Surf., A* **2003**, *229*, 1.
- Fuertes, A. B.; Lotaa, G.; Centenob, T. A.; Frackowiak, E. *Electrochim. Acta* **2005**, *50*, 2799.
- Blin, J. L.; Otjacques, C.; Herrier, G.; Su, B. *Langmuir* **2000**, *16*, 4229.
- Branton, P. J.; Doughert, J.; Lockhart, G.; White, J. W. *Character Porous Solids IV* **1997**, 668.
- Kimura, T.; Sugahara, Y.; Kuroda, K. *Chem. Commun.* **1998**, 559.
- Hwang, Y. K.; Patil, K. R.; Jung, S. H.; Chang, J.; Ko, Y. J.; Park, S. *Microporous Mesoporous Mater.* **2005**, *78*, 245.
- Kunieda, H.; Ozawa, K.; Huang, K. L. *J. Phys. Chem. B* **1998**, *102*, 831.
- Huang, M. H.; Kartono, F.; Dunn, B.; Zink, J. I. *Chem. Mater.* **2002**, *14*, 5153.
- Hanrahan, J. P.; Copley, M. P.; Ryan, K. M.; Spalding, T. R.; Morris, M. A.; Holmes, J. D. *Chem. Mater.* **2004**, *16*, 424.
- Hanrahan, J. P.; Copley, M. P.; Ziegler, K. J.; Spalding, T. R.; Morris, M. A.; Steytler, D. C.; Heenan, R. K.; Schweins, R.; Holmes, J. D. *Langmuir* **2005**, *21*, 4163.
- Pai, R. A.; Humayun, R.; Schulberg, M. T.; Sengupta, A.; Sun, J.; Watkins, J. J. *Science* **2004**, *303*, 507.
- Gupta, G.; Shah, P. S.; Zhang, X.; Saunders, A. E.; Korgel, B. A.; Johnston, K. P. *Chem. Mater.* **2005**, *17*, 6728.
- Ghosh, K.; Lehmler, H.; Rankin, S. E.; Knutson, B. L. *Langmuir* **2005**, *21*, 6145.
- Beckman, E. J. *J. Supercrit. Fluids* **2004**, *28*, 121.
- Beckman, E. J. *Chem. Commun.* **2004**, 17, 1885.
- Cao, C. T.; Fadeev, A. Y.; McCarthy, T. J. *Langmuir* **2001**, *17*, 757.
- Combes, J. R.; White, L. D.; Tripp, C. P. *Langmuir* **1999**, *15*, 7870.
- Pai, R. A.; Watkins, J. J. *Adv. Mater.* **2006**, *18*, 241.
- Jacobson, G. B.; Lee, C. T. J.; Johnston, K. P. *J. Org. Chem.* **1999**, *64*, 1201.
- Holmes, J. D.; Steytler, D. C.; Rees, G. D.; Robinson, B. H. *Langmuir* **1998**, *14*, 6371.
- Yazdi, A. V.; Beckman, E. J. *Mater. Res.* **1995**, *10*, 530.
- Ji, M.; Chen, X.; Wai, C. M.; Fulton, J. L. *J. Am. Chem. Soc.* **1999**, *121*, 2631.
- McLeod, M. C.; McHenry, R. S.; Beckman, E. J.; Roberts, C. B. *J. Phys. Chem. B* **2003**, *107*, 2693.
- Ye, W.; Keiper, J. S.; DeSimone, J. M.; Chin, J. *Polym. Sci.* **2006**, *24*, 95.
- Eastoe, J.; Dupont, A.; Steytler, D. C. *Curr. Opin. Colloid Interface Sci.* **2003**, *8*, 267.
- Harrison, K.; Goveas, J.; Johnston, K. P.; O'Rear, E. A., III. *Langmuir* **1994**, *10*, 3536.
- Lee, C. T., Jr.; Johnston, K. P.; Dai, H. J.; Cochran, H. D.; Melnichenko, Y. B.; Wignall, G. D. *J. Phys. Chem. B* **2001**, *105*, 3540.
- Keiper, J. S.; Simhan, R.; DeSimone, J. M.; Wignall, G. D.; Melnichenko, Y. B.; Frielinghaus, H. J. *Am. Chem. Soc.* **2002**, *124*, 1834.
- da Rocha, S. R. P.; Johnston, K. P.; Rossky, P. J. *J. Phys. Chem. B* **2002**, *106*, 13250.
- Sagisaka, M.; Fujii, T.; Ozaki, Y.; Yoda, S.; Takebayashi, Y.; Kondo, Y.; Yoshino, N.; Sakai, H.; Abe, M.; Otake, K. *Langmuir* **2004**, *20*, 2560.
- Dickson, J. L.; Smith, P. G.; Dhanuka, V. V.; Srinivasan, V.; Stone, M. T.; Rossky, P. J.; Behles, J. A.; Keiper, J. S.; Xu, B.; Johnson, C.; DeSimone, J. M.; Johnston, K. P. *Ind. Eng. Chem. Res.* **2005**, *44*, 1370.
- da Rocha, S. R. P.; Harrison, K.; Johnston, K. P. *Langmuir* **1999**, *15*, 419.
- Psathas, P.; Sander, E. A.; Ryoo, W.; Mitchell, D.; Lagow, R. J.; Lim, K. T.; Johnston, K. P. *J. Dispersion Sci. Technol.* **2002**, *23*, 81.
- Asakawa, T.; Hisamatsu, H.; Miyagishi, S. *Langmuir* **1995**, *11*, 478.
- Tan, B.; Vyas, S. M.; Lehmler, H. J.; Knutson, B. L.; Rankin, S. E. *Chem. Mater.* **2005**, *17*, 916.
- Lu, Y.; Ganguli, R.; Drewien, C. A.; Anderson, M. T.; Brinker, C. J.; Gong, W.; Guo, Y.; Soye, H.; Dunn, B.; Huang, M. H.; Zink, J. I. *Nature* **1997**, *389*, 364.
- ImageJ *Image processing and analysis in Java*; retrieved Jul 5, 2006, from <http://rsb.info.nih.gov/ij/>.
- Kruk, M.; Jaroniec, M.; Gadkaree, K. P. *Langmuir* **1999**, *15*, 1442.
- Kruk, M.; Jaroniec, M.; Sayari, A. *Langmuir* **1997**, *13*, 6267.
- Wang, K.; Karlsson, G.; Almgren, M.; Asakawa, T. *J. Phys. Chem. B* **1999**, *103*, 9237.
- Bothun, D. G.; Kho, Y. W.; Berberich, J. A.; Shofner, J. P.; Robertson, T.; Tatum, K. J.; Knutson, B. L. *J. Phys. Chem. B* **2005**, *109*, 24495.
- Andreas, J. M.; Hauser, E. A.; Tucker, W. B. *J. Phys. Chem.* **1938**, *42*, 1001.
- Kho, Y. W.; Conrad, D. C.; Knutson, B. L. *Fluid Phase Equilib.* **2003**, *206*, 179.
- Wang, K.; Orädd, G.; Almgren, M.; Asakawa, T.; Bergenståhl, B. *Langmuir* **2000**, *16*, 1042.
- Osei-Prempeh, G.; Lehmler, H.; Rankin, S. E.; Knutson, B. L. *Microporous Mesoporous Mater.* **2005**, *85*, 16.
- Alberius, P. C. A.; Frindell, K. L.; Hayward, R. C.; Kramer, E. J.; Stucky, G. D.; Chmelka, B. F. *Chem. Mater.* **2002**, *14*, 3284.
- Klotz, M.; Ayril, A.; Guizard, C.; Cot, L. *J. Mater. Chem.* **2000**, *10*, 663.
- Rankin, S. E.; Tan, B.; Lehmler, H.; Hindman, K. P.; Knutson, B. L. *Microporous Mesoporous Mater.* **2004**, *73*, 197.
- SPARTAN, student version; Wavefunction, Inc.: Irvine, CA, 1998.
- Cagnol, F.; Grosso, D. *J. Mater. Chem.* **2003**, *13*, 61.
- Ulagappan, N.; Rao, C. N. R. *Chem. Commun.* **1996**, 2759.

- (68) Oates, J. D. *J. Colloid Interface Sci.* **1989**, *131*, 307.
- (69) Lee, C. T., Jr.; Johnston, K. P. *J. Am. Chem. Soc.* **2003**, *125*, 3181.
- (70) Lee, C. T., Jr.; Johnston, K. P. *J. Phys. Chem. B* **2000**, *104*, 4448.
- (71) Wissinger, R. G.; Paulaitis, M. E. *J. Polym. Sci., Polym. Phys. Ed.* **1987**, *25*, 2497.
- (72) Zhang, Y.; Gangwani, K. K.; Lemert, R. M. *J. Supercrit. Fluids* **1997**, *11*, 115.
- (73) Goel, S. K.; Beckman, E. J. *Polymer* **1993**, *34*, 1410.
- (74) Fleming, G. K.; Koros, W. J. *Macromolecules* **1986**, *19*, 2285.
- (75) Sirard, S. M.; Green, P. F.; Johnston, K. P. *J. Phys. Chem. B* **2001**, *105*, 766.
- (76) Ryoo, W.; Webber, S. E.; Johnston, K. P. *Ind. Eng. Chem. Res.* **2003**, *42*, 6348.
- (77) Chun, B.-S.; Wilkinson, G. T. *Ind. Eng. Chem. Res.* **1995**, *34*, 4371.
- (78) Psathas, P.; Sander, E. A.; Lee, M. Y.; Lim, K. T.; Johnston, K. P. *J. Dispersion Sci. Technol.* **2002**, *23*, 65.
- (79) Bancroft, W. D. *J. Phys. Chem.* **1913**, *17*, 501.
- (80) Kahlweit, M. *Microemulsions in Chemical Thermo*; Letcher, T., Ed.; Blackwell: Oxford, U.K., 1999; p 37.
- (81) Stone, M. T.; Smith, P. G.; da Rocha, S. R. P.; Rossky, P. J.; Johnston, K. P. *J. Phys. Chem. B* **2004**, *108*, 1962.
- (82) Hentze, H.; Kaler, E. W. *Chem. Mater.* **2003**, *15*, 708.
- (83) Hentze, H.; Co, C. C.; McKelvey, C. A.; Kaler, E. W. *Top. Curr. Chem.* **2003**, *226*, 197.
- (84) Turner, C.; Topgaard, D.; Sivik, B.; Bergenstahl, B. *Colloids Surf., A* **2003**, *213*, 69.
- (85) Scanu, L. F.; Gubbins, K. E.; Hall, C. K. *Langmuir* **2004**, *20*, 514.
- (86) Eastoe, J.; Dupont, A.; Steytler, D. C. *Curr. Opin. Colloid Interface Sci.* **2003**, *8*, 267.
- (87) NIST Chemistry Webbook *NIST Standard Reference Database Number 69 - March, 2003 Release*; retrieved Aug 5, 2006, from <http://webbook.nist.gov/chemistry/>.